Science Advances
AAAS

advances.sciencemag.org/cgi/content/full/7/24/eabg2418/DC1

Supplementary Materials for

Broadband infrared photodetection using a narrow bandgap conjugated polymer

Jarrett H. Vella, Lifeng Huang, Naresh Eedugurala, Kevin S. Mayer, Tse Nga Ng, Jason D. Azoulay*

*Corresponding author. Email: jason.azoulay@usm.edu

Published 9 June 2021, *Sci. Adv.* **7**, eabg2418 (2021)
DOI: 10.1126/sciadv.abg2418

This PDF file includes:

Supplementary Text

Materials and Methods

All manipulations of air- and moisture-sensitive compounds were performed under an inert atmosphere using standard glovebox and Schlenk techniques. Reagents, unless otherwise specified, were purchased from Sigma-Aldrich and used without further purification. 1,1,2,2-Tetrachloroethane-d_2 and chloroform-*d* were purchased from Cambridge Isotope Laboratories and used as received. Tetrakis(triphenylphosphine)palladium(0) and aluminum trichloride ($AlCl_3$) were purchased from Strem Chemicals and used as received. 4*H*-cyclopenta-[2,1-*b*:3,4-*b*']dithiophene (CPDT), 4,4-dimethyl-4*H*-cyclopenta[2,1-*b*:3,4-*b*']dithiophene (*41*), (4,4-dimethyl-4*H*-cyclopenta[2,1-*b*:3,4-*b*']dithiophene-2,6-diyl)bis(trimethylstannane) (**M1**) (*41*), 4,7-dibromobenzo[*c*][1,2,5]thiadiazole-5,6-diamine (*42*), and 2-hexadecylthiophene (*43*) were prepared according to literature procedures.

^1H and ^{13}C NMR spectra were collected on a Bruker Avance III 600 MHz spectrometer and chemical shifts, δ (ppm), were referenced to the residual solvent impurity peak of the solvent. Data are reported as: s = singlet, d = doublet, t = triplet, m = multiplet, br = broad, and coupling constants (*J*) are reported in Hz. Flash chromatography was performed on a Teledyne Isco CombiFlash Purification System using Redi*Sep* Rf prepacked columns. Microwave-assisted reactions were performed in a CEM Discover SP microwave reactor. The number average molecular weight (M_n) and dispersity (*Đ*) were determined by gel permeation chromatography (GPC) relative to polystyrene standards at 160 °C in 1,2,4-trichlorobenzene (stabilized with 125 ppm of BHT) in an Agilent PL-GPC 220 high temperature GPC/SEC system using a set of four PLgel 10 μm MIXED-

B columns. Polymer samples were pre-dissolved at a concentration of 1–2 mg ml^{-1} in 1,2,4-trichlorobenzene with stirring for 4 hours at 160 °C.

Complex Synthesis

1,2-bis(5-hexadecylthiophen-2-yl)ethane-1,2-dione (1). Anhydrous methylene chloride (50 ml) was added to $AlCl_3$ (8.17 g, 61.25 mmol) under nitrogen and stirred to disperse the contents. The mixture was then cooled to –10 °C and oxalyl chloride (1.74 g, 13.7 mmol) was added dropwise. After addition, the mixture was stirred for an additional 15 minutes and a solution of 2-hexadecylthiophene (9.00 g, 29.2 mmol) and pyridine (2.13 g, 27.0 mmol) in methylene chloride (15 ml) was added dropwise using an addition funnel. The reaction mixture was allowed to slowly warm to room temperature. After reaching room temperature, the reaction was quenched with ice, resulting in precipitation of a solid material. The solid precipitate was collected by vacuum filtration and recrystallized from 2-propanol affording 17.22 g of a yellow crystalline solid (25.7 mmol, 88%). Data are as follows: ^{1}H NMR (600 MHz, chloroform-*d*): δ 7.87 (2H, d, *J* = 3.9 Hz), 6.88 (2H, d, *J* = 3.9 Hz), 2.88 (4H, t, *J* = 7.6 Hz), 1.72 (4H, p, *J* = 7.6 Hz), 1.37 (4H, br), 1.26 (50H, s), 0.88 (6H, t, *J* = 6.9Hz). ^{13}C NMR (151 MHz, chloroform-*d*): δ 182.74, 160.19, 137.87, 136.68, 126.54, 32.09, 31.44, 30.99, 29.84, 29.65, 29.52, 29.44, 29.19, 22.84, 14.26. Mass spectrometry (MS) [electrospray ionization (ESI)] exact mass calculated for $C_{42}H_{70}O_2S_2$ is as follows: m/z 671.4890 ($[M^+]$ + $[H^+]$) and 671.4884 (found).

4,9-dibromo-6,7-bis(5-hexadecylthiophen-2-yl)-[1,2,5]thiadiazolo[3,4-*g*]quinoxaline (M2). 1,2-bis(5-hexadecylthiophen-2-yl)ethane-1,2-dione (**1**) (1.24 g, 1.85 mmol), 4,7-dibromobenzo[*c*][1,2,5]thiadiazole-5,6-diamine (1.20 g, 3.70 mmol), and 80 ml of an acetic

acid:chloroform solution (5:1) were combined in a Schlenk flask equipped with a stir bar. The mixture was vigorously purged with nitrogen for 5 minutes and then sealed. The mixture was heated to 70 °C and stirred over the course of 5 days. After cooling to room temperature, the mixture was poured into methanol (15 ml). The resulting precipitate was collected by vacuum filtration and residual solvents were removed *in vacuo*. Purification by flash chromatography using a hexanes:methylene chloride (20:1) gave 613 mg of red solid (0.639 mmol, 35%). Data are as follows: ^{1}H NMR (600 MHz, chloroform-*d*): δ 7.53 (2H, d, *J* = 3.8 Hz), 6.77 (2H, d, *J* = 3.8 Hz), 2.90 (4H, t, *J* = 7.7 Hz), 1.78 (4H, p, *J* = 7.6 Hz), 1.43 (4H, br), 1.26 (50H, s), 0.88 (6H, t, *J* = 6.9Hz). ^{13}C NMR (151 MHz, chloroform-*d*): δ 154.51, 152.42, 148.96, 139.00, 137.85, 132.53, 125.44, 112.61, 32.08, 31.62, 30.82, 29.86, 29.83, 29.81, 29.71, 29.51, 29.39, 22.84, 14.26. Mass spectrometry (MS) [electrospray ionization (ESI)] exact mass calculated for $C_{48}H_{70}Br_2N_4S_3$ is as follows: m/z 957.3208 ($[M^+] + [H^+]$) and 957.3211 (found).

Poly(4-(4,4-dimethyl-4*H*-cyclopenta[2,1-*b*:3,4-*b*']dithiophen-2-yl)-6,7-bis(5-hexadecylthiophen-2-yl)-[1,2,5]thiadiazolo[3,4-*g*]quinoxaline). A microwave tube was charged with **M1** (0.106 mmol, 1.05 equiv) and **M2** (0.101 mmol, 1.0 equiv) The tube was brought inside a nitrogen filled glovebox, and 400 µl of a $Pd(PPh_3)_4$/xylenes stock solution (3.5 mol %) was added followed by an additional 400 µl xylenes. The tube was sealed and subjected to the following reaction conditions in a microwave reactor with stirring: 120 °C for minutes, 140 °C for 5 minutes, and 170 °C for 30 minutes. After this time, the reaction was allowed to cool, leaving a solid gelled material. The mixture was precipitated into methanol and collected via filtration. The residual solid was loaded into an extraction thimble and washed successively (under an nitrogen atmosphere and in the absence of light) with methanol (2 hours), acetone (2 hours), hexanes (2 hours), a 1:4 mixture

of hexanes and tetrahydrofuran (12 hours), and then acetone (2 hours). The polymer was dried *in vacuo* to give 78.3 mg (54 %) of a black solid. Data are as follows: M_n = 20.6 kg mol^{-1} and $Đ$ = 2.54; ^{1}H NMR (600 MHz, 1,1,2,2-tetrachloroethane-d_2, 413 K): δ 9.14 (1H, br), 7.67 (1H, br), 6.93 (1H, br), 3.07 (4H, br), 1.95 (4H, br), 1.34 (56H, br), 0.95 (6H, br).

UV-Vis-NIR and FTIR Spectroscopy

UV-Vis-NIR and Fourier transform infrared (FTIR) spectra were recorded from 0.375 to 3.30 μm and from 3.30 to 16.40 μm using a Cary 5000 UV-Vis-NIR spectrometer and Bruker VERTEX 80 FTIR spectrometer, respectively. Thin films were prepared by spin-coating a chlorobenzene solution (10 mg ml^{-1}) onto quartz or NaCl substrates at 1000 rpm. Absorption: λ_{max} (thin film) = 1.67 μm, ε = 21700 L mol^{-1} cm^{-1}.

Electrochemistry

Electrochemical characteristics were determined by cyclic voltammetry (50 mV s^{-1}) carried out on drop-cast polymer films at room temperature in degassed anhydrous acetonitrile with tetrabutylammonium hexafluorophosphate (0.1 M) as the supporting electrolyte. The working electrode was a platinum wire, the counter electrode was a platinum wire and the reference electrode was Ag/AgCl. After each measurement, the reference electrode was calibrated with ferrocene and the potential axis was corrected to the normal hydrogen electrode (NHE) using −4.75 eV for NHE (*34*). The highest occupied molecular orbital energy level (E_{HOMO}) was estimated as −4.41 eV from the onset of oxidation, and the lowest unoccupied molecular orbital energy level (E_{LUMO}) was estimated as −4.03 eV from the onset of reduction. The electrochemical band gap was calculated as 0.38 eV from the difference between E_{HOMO} and E_{LUMO}.

Grazing-Incidence Wide-Angle X-ray Scattering (GIWAXS)

GIWAXS samples were prepared by spin-coating a film from chlorobenzene (as previously described) onto a Si wafer. The samples were measured at beamline 11-3 of Stanford Synchrotron Radiation Lightsource (SSRL), in a helium-filled chamber, with an incident beam energy of 12.73 keV, and an incident angle of 0.12°. The data were collected on a Rayonix Mar CCD225 detector with a sample to detector distance of 300 mm. An X-ray beam wavelength of 0.9758 Å and an exposure time of 400 s were used. The data were analyzed using WaveMetrics Igor Pro with a Nika script and WAXStools software.

Electron Paramagnetic Resonance (EPR) Spectroscopy

Room temperature continuous-wave EPR spectra were recorded on a Bruker EMXmicro EPR spectrometer operating at X-band. Solid-state samples were loaded into 4 mm quartz tubes and evacuated to 40 mbar for 12 hours before flame sealing under vacuum. Spin concentrations was obtained by comparison against a 2,2-diphenyl-1-picrylhydrazyl standard with a known spin concentration. Variable-temperature measurements were performed on a Bruker E540 or E680 EPR spectrometer operating at X-band. The EPR signal intensity from 25 to 5 K was utilized to extract the singlet–triplet energy splitting (ΔE_{ST}) through fitting the data to the Bleaney–Bowers equation (S1) (*44*):

$$I_{EPR} = \frac{C}{T}\frac{3e^{-2J/k_B T}}{1+3e^{-2J/k_B T}} \quad \text{(S1)}$$

where C is a constant, J is the intramolecular exchange coupling constant, and $2J$ is ΔE_{ST}. The fit parameters, $J = 1.60$ cm^{-1} and $\Delta E_{ST} = 9.15 \times 10^{-3}$ kcal mol^{-1} were obtained.

Conductivity Measurements of Polymer Films

Synthetic quartz-coated glass substrates were sequentially cleaned using 2% Hellmanex detergent in DI water, DI water, acetone, and isopropyl alcohol for 10 min using sonication, followed by drying in an oven. The substrates were then treated in a UV-ozone cleaner for 30 minutes. Gold electrodes (60 nm) were thermally evaporated at 1×10^{-7} torr using a shadow mask. The electrodes were separated by a 60 μm × 1 mm spacing. The polymer was dissolved in chloroform at 58 °C to make 10 mg ml^{-1} or 30 mg ml^{-1} solutions in an N_2 atmosphere. The 10 mg ml^{-1} polymer solution was spin coated onto the substrate at 1000 rpm for 60 seconds resulting in a 76 nm thick film. The 30 mg ml^{-1} polymer solution was spin coated onto the substrate at 600 rpm for 60 seconds resulting in a 1078 nm thick film. Conductivity was measured using a probe station (Signatone 1160 series) inside a nitrogen filled glovebox and the data were recorded on a Keithley 4200 semiconductor characterization system. The conductivity measurements were conducted using a two-point probe method (source and drain, without gate) by sweeping the voltage from –2 to 2 V. The conductivity was determined from the following relationship

$$\sigma = \frac{I}{V} \times \frac{L}{WT} \tag{S2}$$

where σ, I, V, L, W, and T represent conductivity, current, voltage, channel length, channel width, and polymer layer thickness (measured by AFM), respectively (*34*).

Detector Figures of Merit

The responsivity of fully packaged detectors $\Re(\lambda_c, f)$ was calculated using equation S3 (*2*). This is a standard formula used to calculate detector responsivity using a blackbody source chopped at

frequency f and is essentially photocurrent i divided by the optical power emitted by the blackbody impinging the detector active area

$$\Re(\lambda_c, f) = \frac{i}{\left(\frac{hc}{\lambda_c}\right)\left[\int_0^{\lambda_c} \frac{2c\pi}{\lambda^4\left(e^{hc/\lambda kT}-1\right)} d\lambda\right]\left(\frac{A_s A_d}{\pi r^2}\right) t F_F} \tag{S3}$$

where h is Planck's constant, c is the speed of light, λ_c is the detector cutoff wavelength, k is the Boltzmann constant, T is the temperature, A_s is the source area, A_d is the detector area, t is the aperture transmittance, r is the source-to-detector distance, and F_F is the chopper form factor for conversion of peak-to-peak to rms. The first term of the denominator in brackets is recognizable as photon energy at the detector cutoff wavelength λ_c. The second term represents the exitance of a blackbody in units of: photons sr^{-1} s^{-1} cm^{-2} μm^{-1}. Finally, the third term is a testing-setup specific factor describing the source–detector testing geometry. For reference, the blackbody power incident on the detector active area, calculated using the denominator of (S3), is 4.89 nW without a spectral filter (broadband), 2.17 nW for the SWIR filter, 1.55 nW for the MWIR filter, and 0.255 nW for the LWIR filter. Measurable photocurrent within these spectral regions is consistent with the high D^* obtained and is comparable to other highly optimized detector technologies.

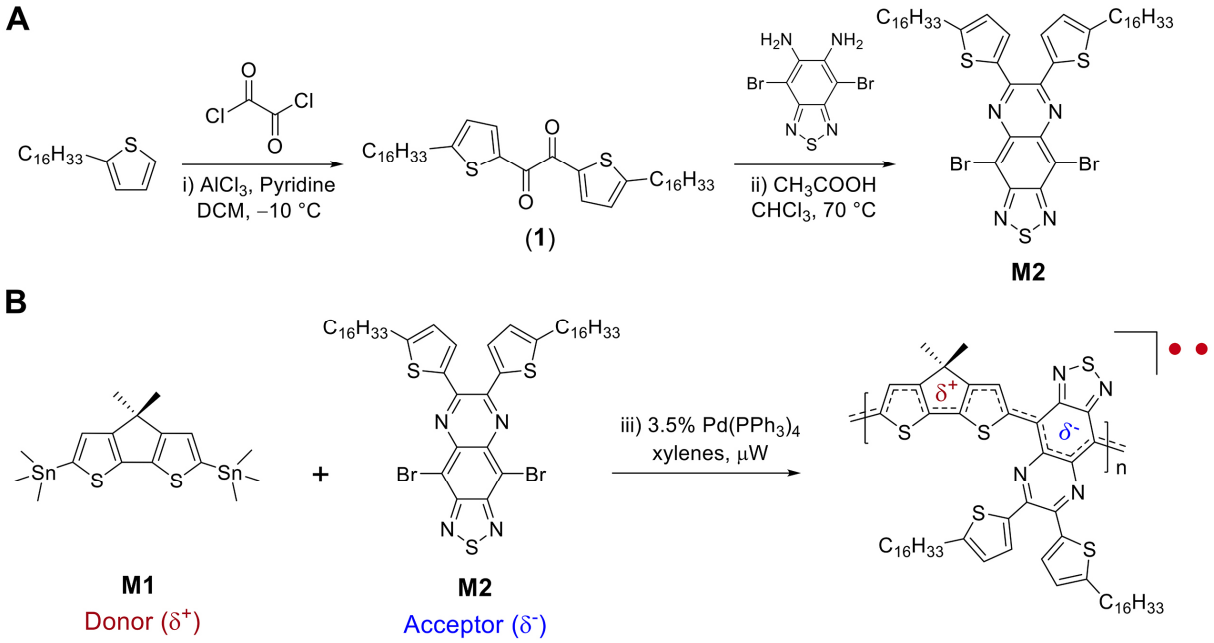

Fig. S1. Monomer and polymer synthesis. (**A**) Synthesis of 1,2-bis(5-hexadecylthiophen-2-yl)ethane-1,2-dione (**1**) and 4,9-dibromo-6,7-bis(5-hexadecylthiophen-2-yl)-[1,2,5]thiadiazolo[3,4-*g*]quinoxaline (**M2**). (**B**) Synthesis of the polymer using a microwave mediated Stille cross-coupling copolymerization between **M1** and **M2**.

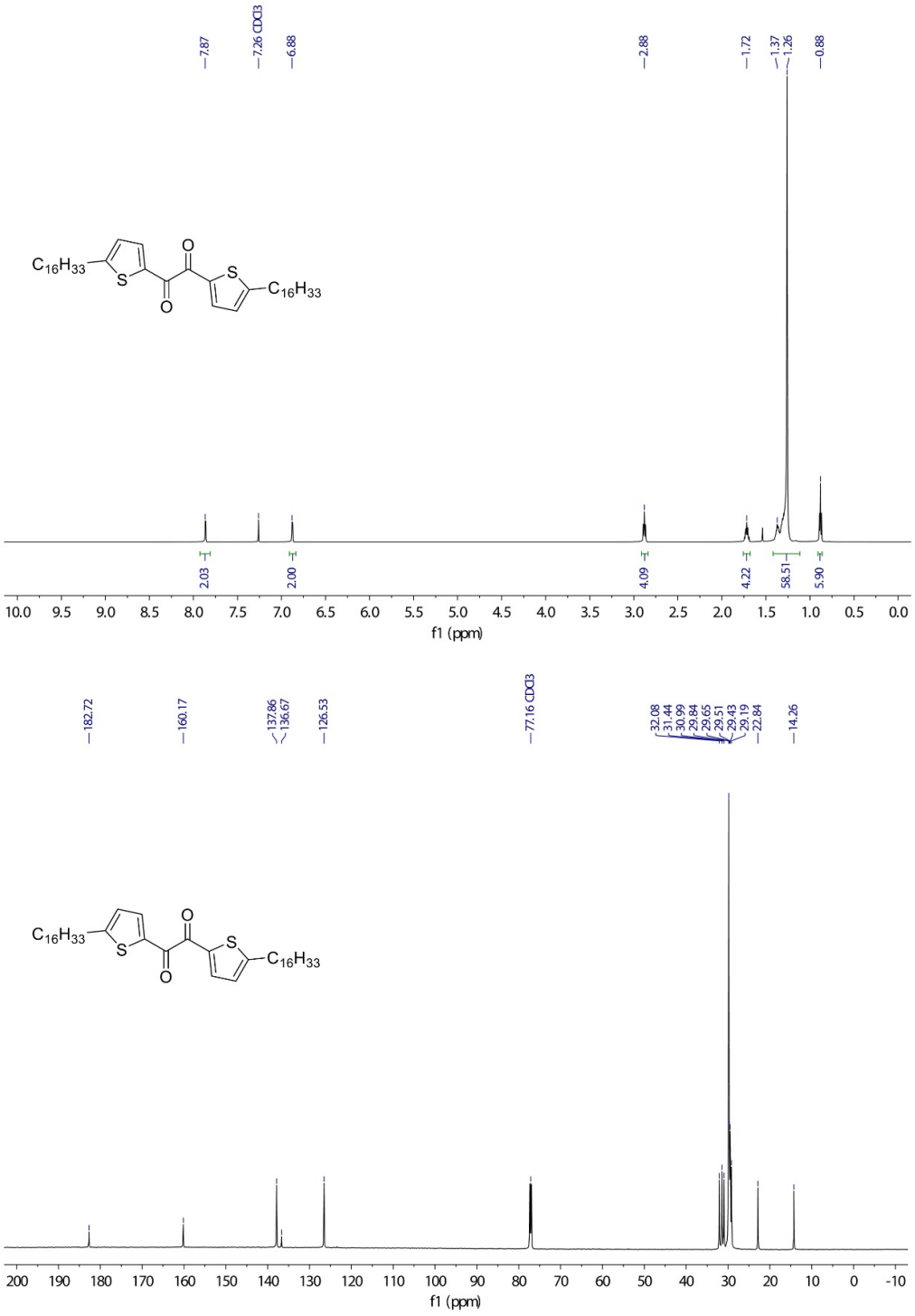

Fig. S2. ^{1}H and ^{13}C NMR spectra of compound 1. (**Top**) ^{1}H NMR spectrum (600 MHz, chloroform-*d*) of 1,2-bis(5-hexadecylthiophen-2-yl)ethane-1,2-dione. (**Bottom**) ^{13}C NMR spectrum (151MHz, chloroform-*d*) of 1,2-bis(5-hexadecylthiophen-2-yl)ethane-1,2-dione.

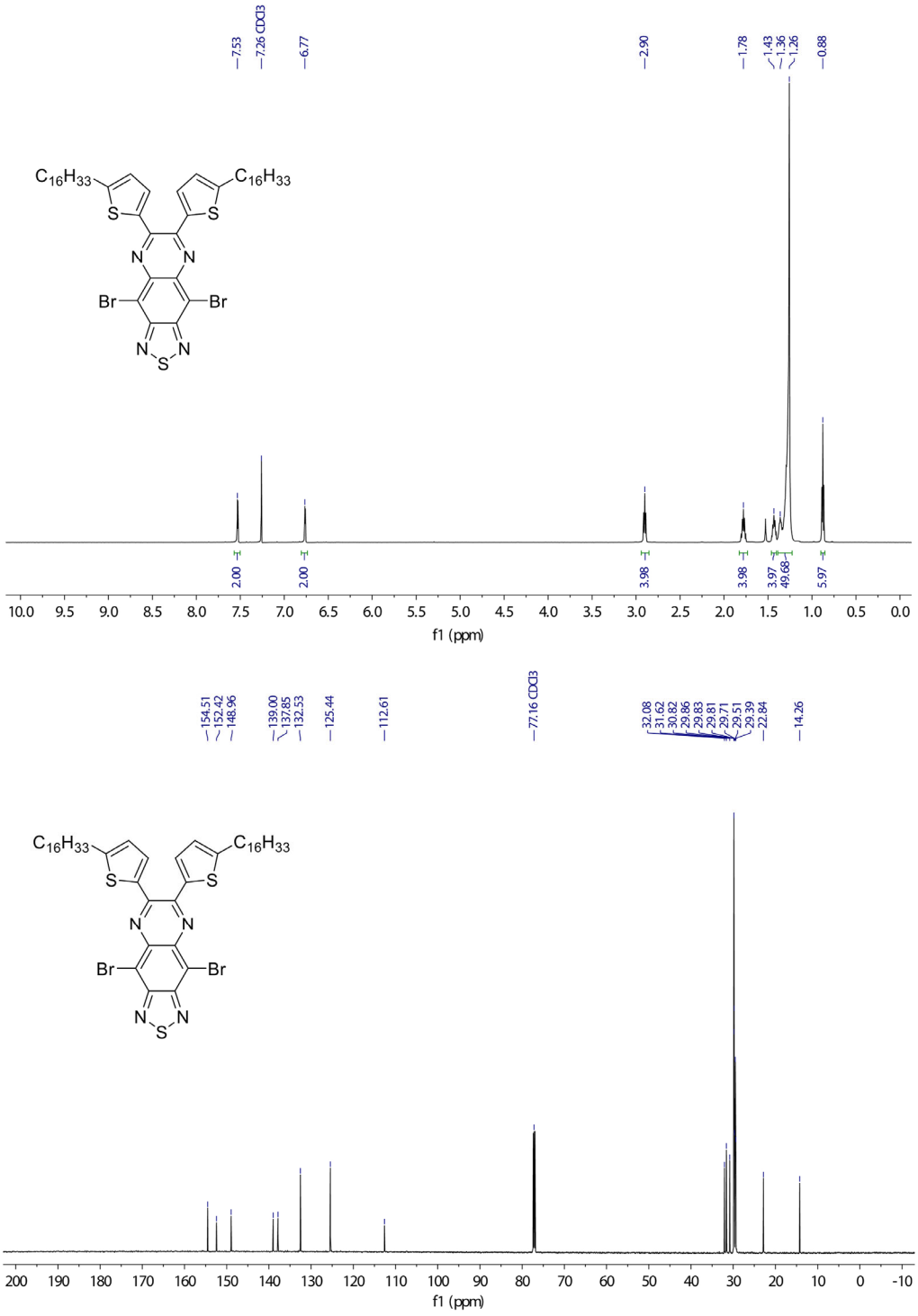

Fig. S3. ^{1}H and ^{13}C NMR spectra of compound M2. (**Top**) ^{1}H NMR spectrum (600 MHz, chloroform-*d*) of 4,9-dibromo-6,7-bis(5-hexadecylthiophen-2-yl)-[1,2,5]thiadiazolo[3,4-*g*]quinoxaline. (**Bottom**) ^{13}C NMR spectrum (151MHz, chloroform-*d*) of 4,9-dibromo-6,7-bis(5-hexadecylthiophen-2-yl)-[1,2,5]thiadiazolo[3,4-*g*]quinoxaline.

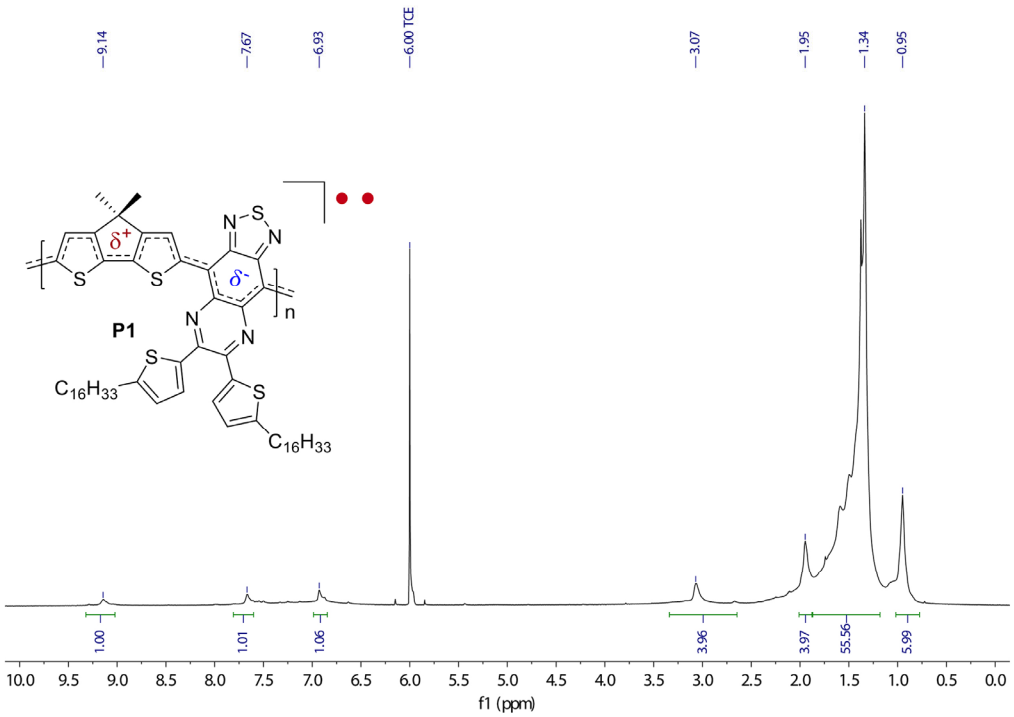

Fig. S4. ^{1}H NMR spectrum of the polymer. ^{1}H NMR spectrum (600 MHz, $C_2D_2Cl_4$, 413 K) of poly(4-(4,4-dimethyl-4*H*-cyclopenta[2,1-*b*:3,4-*b*']dithiophen-2-yl)-6,7-bis(5-hexadecylthiophen-2-yl)-[1,2,5]thiadiazolo[3,4-*g*]quinoxaline).

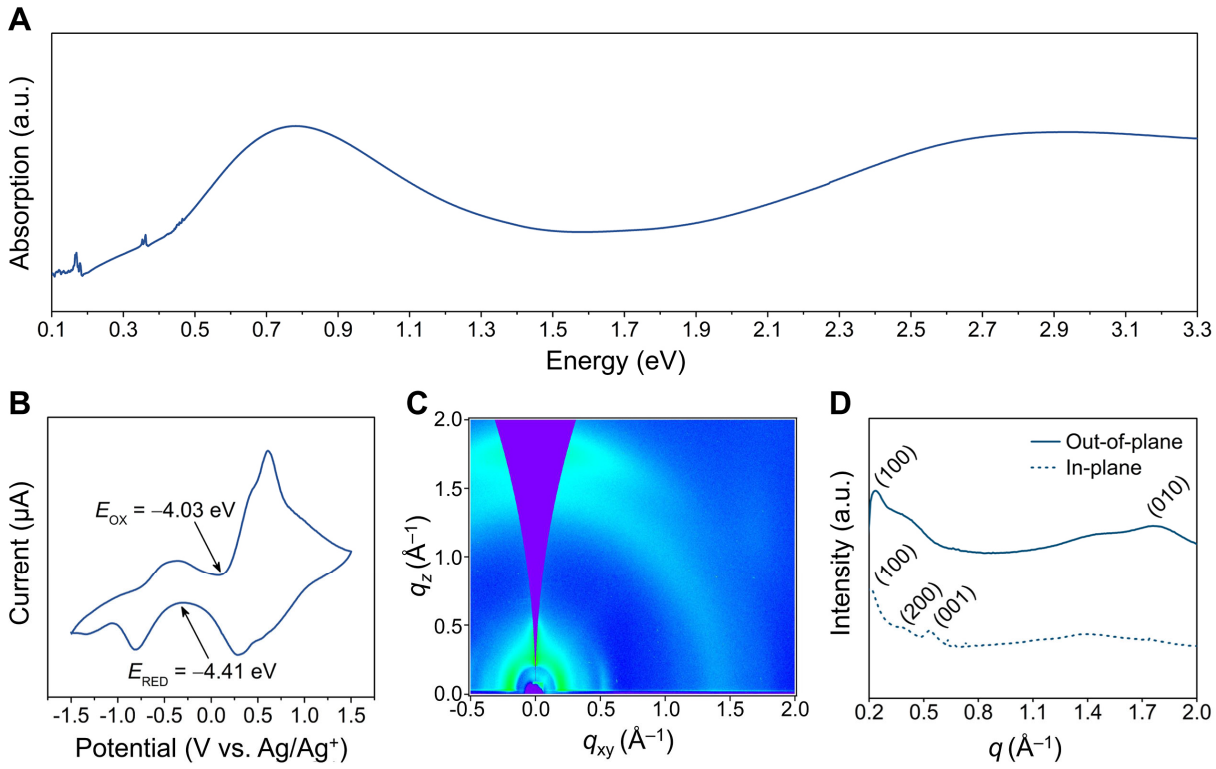

Fig. S5. Solid-state properties of polymer thin films. (**A**) Absorption spectra of thin film cast from chloroform onto quartz and NaCl substrates. (**B**) Cyclic voltammetry indicates an electrochemical bandgap of ~0.38 eV. (**C**) Two-dimensional line cuts of the integrated in-plane and out-of-plane GIWAXS profiles. The weakly ordered sidechain lamellar stacking is indicated by (100) and (200) scattering peaks at q (~0.19 Å^{-1}, ~33.1 Å) and (~0.38 Å^{-1}, ~16.5 Å), respectively. The in-plane (001) peak at q ~ 0.54 Å^{-1} (d ~ 11.6 Å) can be attributed to the polymer backbone packing. The out-of-plane peak at q ~ 1.77 Å^{-1} corresponds to an intermolecular ordering (π–π stacking) distance of ~3.55 Å with a face-on arrangement. (**D**) The corresponding one-dimensional GIWAXS profile.

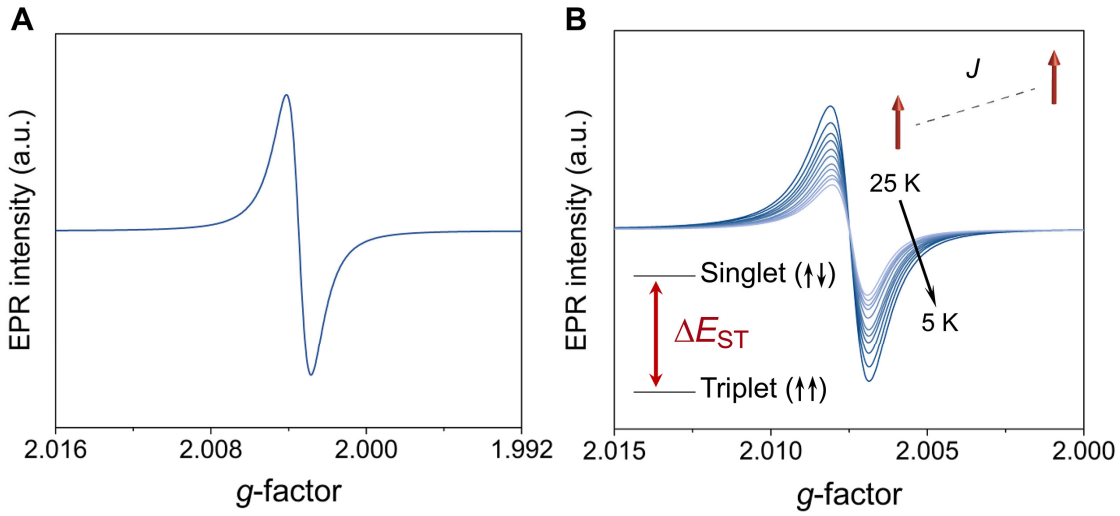

Fig. S6. Electron paramagnetic resonance spectra. (**A**) Solid-state EPR (X-band) spectrum of the polymer at room temperature. (**B**) EPR spectra of the polymer from 25 to 5 K used for the temperature-dependent fit to the Bleaney–Bowers equation with a singlet–triplet energy splitting (ΔE_{ST}) of 9.15×10^{-3} kcal mol^{-1}. The inset is an illustration of intramolecular exchange coupling (J) and ΔE_{ST}.

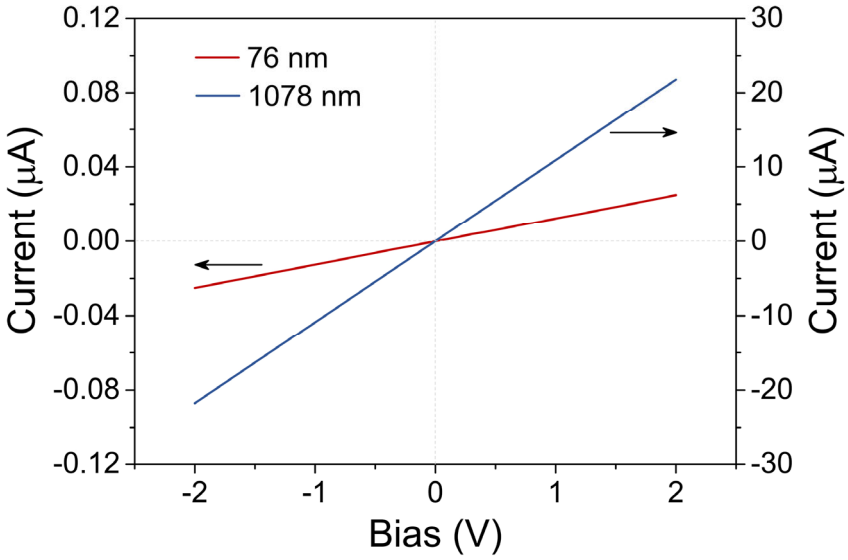

Fig. S7. Current–voltage characteristics of polymer films. Current-voltage characteristics in a 60-μm channel for 76 nm and 1078 nm films with $\sigma = 9.72 \times 10^{-5}$ S cm^{-1} and 5.68×10^{-3} S cm^{-1}, respectively.

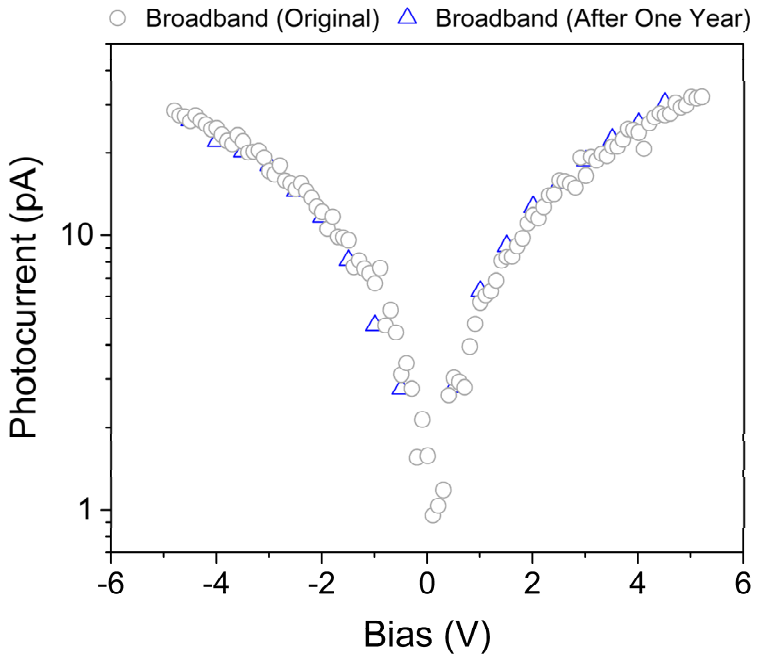

Fig. S8. Stability study of the device. Measurement of the broadband photoconductivity showed no discernable changes over a period of one year.

REFERENCES AND NOTES

1. A. Rogalski, *Infrared and Terahertz Detectors* (CRC Press, 2019).

2. E. L. Dereniak, G. D. Boreman, *Infrared Detectors and Systems* (Wiley, 1996).

3. W. Lei, J. Antoszewski, L. Faraone, Progress, challenges, and opportunities for HgCdTe infrared materials and detectors. *Appl. Phys. Rev.* **2**, 041303 (2015).

4. A. Rogalski, J. Antoszewski, L. Faraone, Third-generation infrared photodetector arrays. *J. Appl. Phys.* **105**, 091101 (2009).

5. P. Martyniuk, J. Antoszewski, M. Martyniuk, L. Faraone, A. Rogalski, New concepts in infrared photodetector designs. *Appl. Phys. Rev.* **1**, 041102 (2014).

6. A. Rogalski, P. Martyniuk, M. Kopytko, InAs/GaSb type-II superlattice infrared detectors: Future prospect. *Appl. Phys. Rev.* **4**, 031304 (2017).

7. M. Richter, T. Heumüller, G. J. Matt, W. Heiss, C. J. Brabec, Carbon photodetectors: The versatility of carbon allotropes. *Adv. Energy Mater.* **7**, 1601574 (2017).

8. B. Y. Zhang, T. Liu, B. Meng, X. Li, G. Liang, X. Hu, Q. J. Wang, Broadband high photoresponse from pure monolayer graphene photodetector. *Nat. Commun.* **4**, 1811 (2013).

9. A. Rogalski, M. Kopytko, P. Martyniuk, Two-dimensional infrared and terahertz detectors: Outlook and status. *Appl. Phys. Rev.* **6**, 021316 (2019).

10. F. Wang, Z. Wang, L. Yin, R. Cheng, J. Wang, Y. Wen, T. A. Shifa, F. Wang, Y. Zhang, X. Zhan, J. He, 2D library beyond graphene and transition metal dichalcogenides: A focus on photodetection. *Chem. Soc. Rev.* **47**, 6296–6341 (2018).

11. M. Long, A. Gao, P. Wang, H. Xia, C. Ott, C. Pan, Y. Fu, E. Liu, X. Chen, W. Lu, T. Nilges, J. Xu, X. Wang, W. Hu, F. Miao, Room temperature high-detectivity mid-infrared photodetectors based on black arsenic phosphorus. *Sci. Adv.* **3**, e1700589 (2017).

12. G. Simone, M. J. Dyson, S. C. J. Meskers, R. A. J. Janssen, G. H. Gelinck, Organic photodetectors and their application in large area and flexible image sensors: The role of dark current. *Adv. Funct. Mater.* **30**, 1904205 (2020).

13. F. P. García de Arquer, A. Armin, P. Meredith, E. H. Sargent, Solution-processed semiconductors for next-generation photodetectors. *Nat. Rev. Mater.* **2**, 16100 (2017).

14. K.-J. Baeg, M. Binda, D. Natali, M. Caironi, Y.-Y. Noh, Organic light detectors: Photodiodes and phototransistors. *Adv. Mater.* **25**, 4267–4295 (2013).

15. Z. Wu, Y. Zhai, H. Kim, J. D. Azoulay, T. N. Ng, Emerging design and characterization guidelines for polymer-based infrared photodetectors. *Acc. Chem. Res.* **51**, 3144–3153 (2018).

16. C. Wang, X. Zhang, W. Hu, Organic photodiodes and phototransistors toward infrared detection: Materials, devices, and applications. *Chem. Soc. Rev.* **49**, 653–670 (2020).

17. Y. Xu, Q. Lin, Photodetectors based on solution-processable semiconductors: Recent advances and perspectives. *Appl. Phys. Rev.* **7**, 011315 (2020).

18. L. Dou, Y. Yang, J. You, Z. Hong, W.-H. Chang, G. Li, Y. Yang, Solution-processed hybrid perovskite photodetectors with high detectivity. *Nat. Commun.* **5**, 5404 (2014).

19. S. B. Hafiz, M. Scimeca, A. Sahu, D.-K. Ko, Colloidal quantum dots for thermal infrared sensing and imaging. *Nano Converg.* **6**, 7 (2019).

20. G. Konstantatos, I. Howard, A. Fischer, S. Hoogland, J. Clifford, E. Klem, L. Levina, E. H. Sargent, Ultrasensitive solution-cast quantum dot photodetectors. *Nature* **442**, 180–183 (2006).

21. M. Long, Y. Wang, P. Wang, X. Zhou, H. Xia, C. Luo, S. Huang, G. Zhang, H. Yan, Z. Fan, X. Wu, X. Chen, W. Lu, W. Hu, Palladium diselenide long-wavelength infrared photodetector with high sensitivity and stability. *ACS Nano* **13**, 2511–2519 (2019).

22. L. Dou, Y. Liu, Z. Hong, G. Li, Y. Yang, Low-bandgap near-IR conjugated polymers/molecules for organic electronics. *Chem. Rev.* **115**, 12633–12665 (2015).

23. J.-L. Hou, A. Fischer, S.-C. Yang, J. Benduhn, J. Widmer, D. Kasemann, K. Vandewal, K. Leo, Plasmon-induced sub-bandgap photodetection with organic Schottky diodes. *Adv. Funct. Mater.* **26**, 5741–5747 (2016).

24. B. Siegmund, A. Mischok, J. Benduhn, O. Zeika, S. Ullbrich, F. Nehm, M. Böhm, D. Spoltore, H. Fröb, C. Körner, K. Leo, K. Vandewal, Organic narrowband near-infrared photodetectors based on intermolecular charge-transfer absorption. *Nat. Commun.* **8**, 15421 (2017).

25. W. Yao, Z. Wu, E. Huang, L. Huang, A. E. London, Z. Liu, J. D. Azoulay, T. N. Ng, Organic bulk heterojunction infrared photodiodes for imaging out to 1300 nm. *ACS Appl. Electron. Mater.* **1**, 660–666 (2019).

26. X. Gong, M. Tong, Y. Xia, W. Cai, J. S. Moon, Y. Cao, G. Yu, C.-L. Shieh, B. Nilsson, A. J. Heeger, High-detectivity polymer photodetectors with spectral response from 300 nm to 1450 nm. *Science* **325**, 1665–1667 (2009).

27. A. E. London, L. Huang, B. A. Zhang, M. B. Oviedo, J. Tropp, W. Yao, Z. Wu, B. M. Wong, T. N. Ng, J. D. Azoulay, Donor–acceptor polymers with tunable infrared photoresponse. *Polym. Chem.* **8**, 2922–2930 (2017).

28. A. D. Stiff-Roberts, K. R. Lantz, R. Pate, Room-temperature, mid-infrared photodetection in colloidal quantum dot/conjugated polymer hybrid nanocomposites: A new approach to quantum dot infrared photodetectors. *J. Phys. D Appl. Phys.* **42**, 234004 (2009).

29. M. Zhang, J. T. W. Yeow, A flexible, scalable, and self-powered mid-infrared detector based on transparent PEDOT: PSS/graphene composite. *Carbon* **156**, 339–345 (2020).

30. A. Blaikie, D. Miller, B. J. Alemán, A fast and sensitive room-temperature graphene nanomechanical bolometer. *Nat. Commun.* **10**, 4726 (2019).

31. S. Ebrahim, A. M. Elshaer, M. Soliman, M. B. Tayl, Pyroelectric infrared detector based on polyaniline/polyvinylidene fluoride blend. *Sens. Actuat. A Phys.* **238**, 389–396 (2016).

32. D. B. Sulas, A. E. London, L. Huang, L. Xu, Z. Wu, T. N. Ng, B. M. Wong, C. W. Schlenker, J. D. Azoulay, M. Y. Sfeir, Preferential charge generation at aggregate sites in narrow band gap infrared photoresponsive polymer semiconductors. *Adv. Opt. Mater.* **6**, 1701138 (2018).

33. K. Wang, L. Huang, N. Eedugurala, S. Zhang, M. A. Sabuj, N. Rai, X. Gu, J. D. Azoulay, T. N. Ng, Wide potential window supercapacitors using open-shell donor–acceptor conjugated polymers with stable n-doped states. *Adv. Energy Mater.* **9**, 1902806 (2019).

34. L. Huang, N. Eedugurala, A. Benasco, S. Zhang, K. S. Mayer, D. J. Adams, B. Fowler, M. M. Lockart, M. Saghayezhian, H. Tahir, E. R. King, S. Morgan, M. K. Bowman, X. Gu, J. D. Azoulay, Open-shell donor–acceptor conjugated polymers with high electrical conductivity. *Adv. Funct. Mater.* **30**, 1909805 (2020).

35. A. E. London, H. Chen, M. A. Sabuj, J. Tropp, M. Saghayezhian, N. Eedugurala, B. A. Zhang, Y. Liu, X. Gu, B. M. Wong, N. Rai, M. K. Bowman, J. D. Azoulay, A high-spin ground-state donor–acceptor conjugated polymer. *Sci. Adv.* **5**, eaav2336 (2019).

36. Z. X. Chen, Y. Li, F. Huang, Persistent and stable organic radicals: Design, synthesis, and applications. *Chem* **7**, 288–332 (2021).

37. M. Li, C. An, W. Pisula, K. Müllen, Cyclopentadithiophene–benzothiadiazole donor–acceptor polymers as prototypical semiconductors for high-performance field-effect transistors. *Acc. Chem. Res.* **51**, 1196–1205 (2018).

38. M. Chang, G. T. Lim, B. Park, E. Reichmanis, Control of molecular ordering, alignment, and charge transport in solution-processed conjugated polymer thin films. *Polymers* **9**, 212 (2017).

39. Y. Joo, V. Agarkar, S. H. Sung, B. M. Savoie, B. W. Boudouris, A nonconjugated radical polymer glass with high electrical conductivity. *Science* **359**, 1391–1395 (2018).

40. A. Daniels, *Field Guide to Infrared Systems, Detectors, and FPAs* (SPIE, 2018).

41. M. Wang, M. J. Ford, C. Zhou, M. Seifrid, T.-Q. Nguyen, G. C. Bazan, Linear conjugated polymer backbones improve alignment in nanogroove-assisted organic field-effect transistors. *J. Am. Chem. Soc.* **139**, 17624–17631 (2017).

42. Y. Tsubata, T. Suzuki, Y. Yamashita, T. Mukai, T. Miyashi, Tetracyanoquinodimethanes fused with 1,2,5-thiadiazole and pyrazine units. *Heterocycles* **33**, 337–348 (1992).

43. T. V. Richter, C. H. Braun, S. Link, M. Scheuble, E. J. W. Crossland, F. Stelzl, U. Würfel, S. Ludwigs, Regioregular polythiophenes with alkylthiophene side chains. *Macromolecules* **45**, 5782–5788 (2012).

44. B. Bleaney, Anomalous paramagnetism of copper acetate. *Rev. Mod. Phys.* **25**, 161–162 (1953).